

1 **Size distribution of submarine landslides and its implication to tsunami**
2 **hazard in Puerto Rico**

3
4 Uri S. ten Brink

5 U.S. Geological Survey, Woods Hole, MA 02543 USA

6 Eric L. Geist

7 U.S. Geological Survey, Menlo Park, CA 94025 USA

8 Brian D. Andrews

9 U.S. Geological Survey, Woods Hole, MA 02543 USA

10 **ABSTRACT**

11 **We have established for the first time a size frequency distribution for some**
12 **carbonate submarine slope failures. Using detailed bathymetry along the northern**
13 **edge of the carbonate platform north of Puerto Rico, we show that the cumulative**
14 **distribution of slope failure volumes follows a power law distribution. The power**
15 **law exponent of this distribution is similar to those for rock falls on land,**
16 **commensurate with their interpreted failure mode. The carbonate volume**
17 **distribution and its associated volume-area relationship are significantly different**
18 **from those for clay-rich debris lobes in the Storegga slide, Norway. Coupling this**
19 **relationship with tsunami simulations allows an estimate of the maximum tsunami**
20 **runup and the maximum number of potentially damaging tsunamis from landslides**
21 **to the north shore of Puerto Rico.**

22
23 **INTRODUCTION**

24 The mitigation of earthquake hazard via the modification of building codes is
25 based on probabilistic estimates of ground shaking within a given time period [*Cornell*,
26 1968]. These estimates are based, among other things, on the fact that the frequency of
27 earthquakes as a function of earthquake magnitude follows a power law distribution. This
28 distribution allows us to estimate the number of earthquakes from incomplete
29 observations and is indicative of the fundamental processes behind the generation of
30 earthquakes [e.g., *Rundle et al.*, 2003]. It has been suggested that the area and volume of
31 subaerial landslides also follow a power-law distribution [*Fuyii*, 1969; *Sugai et al.*, 1994;
32 *Dussauge et al.*, 2003; *Malamud et al.*, 2004]. To date only one submarine slope failure
33 distribution was established (clay-rich debris lobes of the Storegga slide, *Issler et al.*,
34 2005), but interest in submarine landslides is increasing because they are known to have
35 generated destructive tsunamis [*Piper et al.*, 1999; *Satake and Tanioka*, 2003; *Ward*,
36 2001; *Lee et al.*, 2003].

37 The north shore of Puerto Rico and its offshore region are covered by thick layers
38 of carbonate rocks that now dip northward at an angle of 4° (Figure 1). These layers were
39 deposited horizontally near sea level, and were tilted about 3.3 Ma, such that their
40 northernmost extent is at a depth of 4000 m and their southern extent on land in Puerto
41 Rico is at a reconstructed elevation (before erosion) of +1300 m [*ten Brink*, 2005]. The
42 tilt episode may have been very short, ≤ 40 kyr [*ten Brink*, 2005]. The tilting has likely
43 increased the probability of seismically induced landslides. Tectonic motions, such as the
44 opening of Mona rift and the subduction of the North American plate, continue to shape
45 the area and generate earthquakes that can trigger landslides. In fact, two devastating

46 tsunamis, associated with moderately large earthquakes, have struck the region north of
47 Puerto Rico and the Dominican Republic during the past 100 years [*Lander et al.*, 2002].

48

49 **SIZE DISTRIBUTION OF SUBMARINE LANDSLIDES**

50 We identified 160 landslide scarps within a 12,000 km² area of the ocean floor
51 along the northern edge of the tilted carbonate platform north of Puerto Rico and the
52 Virgin Island (Figure 1). The scarps were identified by examining perspective views of
53 the bathymetry from different angles and illuminations, together with slope maps and
54 with seismic reflection profiles, which provide vertical cross-sections of the landslides
55 (Figure 1). Criteria for landslide scarps included a steep headwall and a flat or inverse
56 toe, fissures in the carbonate platform in orientations other than that of the dominant
57 drainage system, and perturbations to the regular stratigraphy of the carbonate layers.
58 Landslide volumes were calculated by interpolating smooth surfaces through polygons
59 that define the edges of each slide, gridding these smooth surfaces, and subtracting these
60 grids from the gridded topography of each scarp (Figure 1c). The grid size for both the
61 topography and the smoothed surface is 50 m.

62 The volume distribution of 160 slope failures follows a power law, $N_L = 26 V^{-0.64}$
63 in the volume range of 0.07-20 km³ (Figure 2), where N_L is the cumulative number of
64 failures exceeding a volume, V . The volume distribution of submarine slope failures
65 deviates from a power law for volumes <0.07 km³ (Figure 2), probably because of under-
66 sampling of the many smallest failures, a phenomenon observed in subaerial landslides
67 [*Stark and Hovius*, 2001]. It is therefore, reasonable to assume that hundreds more of
68 small failure scarps exist along the edge of the carbonate platform north of Puerto Rico.

69 However, these hundreds of small slope failures are expected to contribute in total no
70 more than 17 km^3 , or 4% of the expected total volume of landslides. In other words, the
71 few largest failure volumes dominate the retreat process of the edge of the carbonate
72 platform. This conclusion is expressed mathematically by a power law exponent <1 .

73 The two largest observed slope failures have volumes smaller than is predicted by
74 power law relationship. This drop off is best fit by an upper-truncated power-law
75 distribution, though it is unclear if there are physical mechanisms that limit landslide
76 volume (a “corner volume”) or if the roll-off is caused by under-sampling [*Burroughs*
77 *and Tebbens*, 2001]. *Sugai et al.* [1994] noted a similar pattern in landslide distributions
78 in the Akaishi mountains, Japan. If the drop-off is due to under-sampling, the un-
79 truncated power-law would predict an additional slide with a volume of $\sim 107 \text{ km}^3$, almost
80 4 times the largest observed failure volume, but a lot smaller than previously suggested
81 (1500 km^3 [*Schwab et al.*, 1991]; 900 km^3 [*Mercado et al.*, 2002]). These previous
82 suggestions were based on lower resolution bathymetry data, and assumed that a large
83 part or even the entire amphitheater-shaped scarp north of Arecibo (Figure 1) failed at
84 once. However, the failure process appears continuous with recent failures over-printing
85 older ones (Figure 1; *ten Brink et al.*, 2006).

86 *Dussauge et al.* [2003] found that volume distribution of landslides on subvertical
87 cliffs on land that are classified as rock falls [*Varnes*, 1978] can be fit by a power law
88 with an exponent, $b=0.5\pm 0.2$. This distribution is similar to our submarine size
89 distribution, despite its smaller (2-3 orders) volume range. Our submarine slope failures
90 and subaerial landslides also appear similar in their volume-area relationship. This
91 relationship is $V_L=0.024A_L^{1.368}$ for 201 mapped landslides in the mountains of New

92 Guinea [Simonett, 1967], and $V_L=0.0263A_L^{1.292}$ for all submarine slope failures, except 4
93 failure areas that are defined by fissures and lack a clear concave shape (Figure 3).

94 The similarity between the volume distribution of submarine landslides north of
95 Puerto Rico and the distribution of land rock falls may reflect similar underlying physical
96 processes. The landslides are located at the edge of a 1-2 km thick massive and layered
97 limestone [e.g., van Gestel et al., 1999], where slopes exceed 20°. Observations from this
98 area [ten Brink et al., 2006] indicate that slope failures have occurred as rotational
99 slumps, rock slides, and debris avalanches (as classified by Lee et al., [1993]). Densmore
100 et al. [1998] proposed that the probability distribution of subaerial landslide volumes
101 follows a power law distribution with an exponent that depends on the mechanical
102 properties of the rock mass (cohesion and internal friction angle). Their simulations show
103 rocks with lower cohesion or lower friction coefficient to have $b=1.2$, and rocks with
104 higher cohesion or friction coefficient to have $b=0.8$. Indeed, subaerial landslides of less
105 consolidated material on lower slopes appear to have a higher exponent ($b=1.2\pm 0.3$;
106 Dussauge et al., 2003).

107 The similarity between submarine and subaerial landslide distribution may not
108 necessarily extend to other types of slope failures, such as submarine mud flows,
109 turbidity flows, and debris flows (as classified by Lee et al., [1993]), because of the role
110 of aqueous overpressure in marine sediments. The 63 mapped clay-rich debris lobes in
111 the Storegga slide, tabulated by Haflidason et al. [2005], follow almost a linear volume-
112 area relationship ($V_L=0.0267A_L^{1.032}$, $R^2=0.708$, and $V_L=0.0221A_L^{1.017}$, $R^2=0.740$, for their
113 maximum and minimum volume estimates, respectively; Figure S1a). This relationship
114 indicates that the thickness of the sliding layer is on average constant regardless of slide

115 area and is in contrast to the volume/area relationship of Puerto Rico failures, which
116 indicate deeper excavation by larger failures. *Issler et al.*, [2005] proposed a logarithmic
117 size distribution for the Storegga debris lobes, not a power law, although their
118 relationship does not account for the largest lobes (100-1300 km³). However, if we
119 assume undersampling of the smaller lobes (<1 km³), as in Puerto Rico and in subaerial
120 slides, a power Law, $N_L = 39 V^{-0.44}$ can be fit for the 31 largest lobes (Figure S1b). The
121 exponent, 0.44, is significantly lower than in Puerto Rico and land rockfalls, probably
122 because of the different failure process.

123

124 **TSUNAMI SIMULATION**

125 We next model the tsunami runup expected by the largest failure volume (Figure
126 1b), located 35 km north of Arecibo, Puerto Rico, whose internal deformation is revealed
127 by a crossing seismic profile (Figure 1b). A simplified representation of this slope failure
128 is parameterized according to its total length (8 km), which includes 3.5 km of evacuation
129 and 4.5 km of accumulation, and is extended laterally to the width of the observed failure
130 (See Table S1). A landslide volume of 22 km³ is calculated by fitting a smooth surface
131 over the three-dimensional scarp. The landslide is modeled as a region of depletion with a
132 sharp head scarp and a down slope region of deposition, both of nearly equal volumes
133 (Figure 1b; e.g., *Trifunac et al.*, 2003]). Movement of the landslide is specified according
134 to its duration time (t_d) with smooth ramps used to simulate the accelerating (starting) and
135 decelerating (stopping) phases of slide motion. Slide movement is directly coupled with
136 the hydrodynamic equations of motion through temporal and spatial derivatives of

137 seafloor motion. The hydrodynamic modeling is based on weakly nonlinear “extended”
138 equations [*Lynett and Liu, 2002*]. See electronic supplement for further details.

139 The maximum tsunami runup on the north coast of Puerto Rico resulting from the
140 largest observed volume failure is estimated at 15.7 m (Figure 4). We systematically vary
141 the failure volume by varying the failure width and keeping the failure profile and the
142 other parameters constant to derive a relationship between tsunami runup and the failure
143 volume (Figure 4, Table S1). For potentially larger slope failures north of Puerto Rico,
144 such as the one estimated from an un-truncated power-law distribution (107 km^3 , Figure
145 2), the maximum predicted runup is 31 m (Figure 4).

146 We next investigate the smallest failure volume that is capable of generating a
147 damaging tsunami along the north coast of Puerto Rico. There has not been a historical
148 tsunami along this coast, but tsunami runup above 2.5 m along the west coast of Puerto
149 Rico during the 1918 earthquake, resulted in considerable damage and loss of life
150 [*Mercado and McCann, 1998*]. The smallest failure volume that will generate 2.5 m
151 runup on the north coast of Puerto Rico is 5 km^3 . Only 9 out of 160 slope failures have a
152 volume $\geq 5 \text{ km}^3$ (Figure 2). The estimate of the number of devastating tsunamis within
153 the study area is probably realistic, because the morphology of the coast at Arecibo is
154 typical of the north coast of Puerto Rico, and the modeled failure is closer to the coast
155 than all the other mapped slope failures (Figure 1). A recurrence interval for tsunamis
156 cannot be derived presently because the ages of slope failures north of Puerto Rico are
157 unknown.

158 The caveat in these predictions is the fact that the calculated runup is highly
159 dependent on the prescribed duration (or velocity) of the landslide (Figure S2). Various

160 landslides within a single region, or even during the same triggering event may in fact
161 have different durations. The above runup estimates were calculated using an effective
162 slide velocity of 40 m/s, but the runup will be approximately half as high for a velocity of
163 20 m/s. (See electronic supplement for further discussion).

164

165 **Conclusions**

166 We have established for the first time the frequency distribution for carbonate
167 submarine slope failures. The volume distribution of submarine slides at edge of the
168 massive carbonate platform north of Puerto Rico follows a power law. This distribution
169 allows estimates of the total volume of slumped material, and indicates that a few largest
170 failure dominate the failure volume. The power law has the same exponent as that for the
171 distribution of subaerial rockfalls despite differences in scale, indicating similar
172 processes. The carbonate slope failure distribution is contrasted with the distribution of
173 the clay-rich Storegga debris flows, which likely reflect different processes.

174 The submarine failure statistics can be applied to estimates of the impact of
175 landslide-generated tsunamis on the north shore of Puerto Rico. The largest mapped slide
176 moving with an assumed slide speed of ~40 m/s could have caused 15.7 m high runup.
177 Only the largest 9 of 160 mapped slope failures could have caused a tsunami runup
178 higher than 2.5 m. Future dating of the failure scarps will allow us to estimate the
179 tsunami recurrence interval north of Puerto Rico.

180

181 **ACKNOWLEDGEMENTS**

182 We thank VeeAnn Cross for technical assistance and Bill Schwab, David Twichell and

183 Homa Lee, D. Issler, and anonymous for thorough reviews.

184

185 **REFERENCES CITED**

186 Burroughs, S. M., and S. F. Tebbens (2001), Upper-truncated power laws in natural
187 systems, *Pure Appl. Geophys.*, *158*, 741-757.

188 Cornell, C. A. (1968), Engineering seismic risk analysis, *Bull. Seismol. Soc. Am.*, *58*,
189 1583-1606.

190 Densmore, A. L., M. A. Ellis, and R. S. Anderson (1998), Landsliding and the evolution
191 of normal-fault-bounded mountains, *J. Geophys. Res.*, *103*, 15,203-215,219.

192 Dussauge, C., J.-R. Grasso, and A. Helmstetter, (2003), Statistical analysis of rockfall
193 volume distributions; implications for rockfall dynamics, *J. Geophys. Res.*, *108*, 2286,
194 doi:10.1029/2001JB000650.

195 Fuyii, Y. (1969), Frequency distribution of the landslides caused by heavy rain-fall, *J.*
196 *Seismol. Soc. Jpn*, *22*, 244-247.

197 Haflidason, H., R. Lien, H.P. Sejrup, C.F. Forsberg, and P. Bryn, (2005), The dating and
198 morphometry of the Storegga Slide, *Mar. Petrol. Geol.*, *22*, 123-136.

199 Issler, D., F.V. De Blasio, A. Elverhoi, P. Bryn, and R. Lien, (2005), Scaling behaviour
200 of clay-rich submarine debris flows, *Mar. Petrol. Geol.*, *22*, 187-194.

201 Lander, J. F., L.S. Whiteside, and P.A. Lockridge (2002), A brief history of tsunamis in
202 the Caribbean Sea, *Sci. Tsunami Hazards*, *20*, 57-94.

203 Lee, H. J., R.E. Kayen, J.V. Gardner, and J. Locat (2003), Characteristics of several
204 tsunamigenic submarine landslides, in *Submarine mass movements and their*
205 *consequences*, edited by J. Locat and J. Meinart, pp. 357-366, Kluwer, Amsterdam.

206 Lee, H. J., W.C. Schwab, and J.S. Booth (1993), Submarine landslides; an introduction,
207 in *Submarine landslides; selected studies in the U.S. Exclusive Economic Zone*, edited
208 by W. C. Schwab, H J Lee, and D C Twichell, U. S. Geological Survey Bulletin,
209 Report: B 2002.

210 Lynett, P., and P. L.-F. Liu (2002), A Numerical Study of Submarine Landslide
211 Generated Waves and Runup, *Proc. Royal Soc. Lond. A.*, 458, 2885-2910.

212 Malamud, B. D., D.L. Turcotte, F. Guzzetti, and P. Reichenbach (2004), Landslide
213 inventories and their statistical properties, *Earth Surface Processes and Landforms*,
214 29, 687-711.

215 Mercado, A., N.R. Grindlay, P. Lynett, P., and P. L.-F. Liu, (2002), Investigation of the
216 potential tsunami hazard on the north coast of Puerto Rico due to submarine
217 landslides along the Puerto Rico trench, *Report submitted to Puerto Rico State
218 Emergency Management Agency and Sea Grant College Program*, 432 pp.

219 Mercado, A., and W. McCann (1998), Numerical simulation of the 1918 Puerto Rico
220 tsunami, *Natural Hazards*, 18, 57-76.

221 Piper, D. J. W., P. Cochonat, and M.L. Morrison (1999), The sequence of events around
222 the epicentre of the 1929 Grand Banks earthquake; initiation of debris flows and
223 turbidity current inferred from sidescan sonar, *Sedimentology*, 46, 79-97.

224 Rundle, J. B., D.L. Turcotte, R. Shcherbakov, W. Klein, and C. Sammis (2003),
225 Statistical physics approach to understanding the multiscale dynamics of earthquake
226 fault systems, *Rev. Geophys.*, 41, 5.1-5.30.

227 Satake, K., and Y. Tanioka (2003), The July 1998 Papua New Guinea earthquake:
228 Mechanism and quantification of unusual tsunami generation, *Pure Appl. Geophys.*,

229 160, 2087-2118.

230 Schwab, W. C., W. W. Danforth, K. M. Scanlon, and D.G. Masson (1991), A giant
231 submarine slope failure on the northern insular slope of Puerto Rico, *Mar. Geol.*, 96,
232 237-246.

233 Simonett, D. S. (1967), Landslide distribution and earthquakes in the Bewani and
234 Torricelli Mountains, New Guinea, in *Landform studies from Australia and New*
235 *Guinea*, edited by J. N. a. M. Jennings, J.A., Cambridge University Press, Cambridge.

236 Stark, C. P., and N. Hovius (2001), The characterization of landslide size distributions,
237 *Geophys. Res. Lett.*, 28, 1091-1094.

238 Sugai, T., H. Ohmori, and M. Hirano (1994), Rock control on magnitude-frequency
239 distribution of landslides, *Trans. Jpn. Geomorph. Union*, 15, 233-251.

240 ten Brink, U. S. (2005), Vertical motions of the Puerto Rico Trench and their cause, *J.*
241 *Geophys. Res.*, 110, B06404, doi:06410.01020/02004JB003459,.

242 ten Brink, U. S., W.W. Danforth, C. Polloni, B. Andrews, P. Llanes, S.V. Smith, E.
243 Parker, and T. Uozumi (2004), New sea floor map of the Puerto Rico trench helps
244 assess earthquake and tsunami hazards, *EOS*, 85, 349, 354.

245 ten Brink, U. S., E.L. Geist, P. Lynett, and B. Andrews (2006), Submarine slides north of
246 Puerto Rico and their tsunami potential, in *Caribbean Tsunami Hazard*, edited by A.
247 Mercado and P. L.-F. Liu, World Scientific Publishing, Hackensack.

248 Trifunac, M. D., A. Hayir, and M.I. Todorovska (2003), A note on tsunami caused by
249 submarine slides and slumps spreading in one dimension with nonuniform
250 displacement amplitudes, *Soil Dynamics and Earthquake Engineering*, 23, 223-234.

251 van Gestel, J.-P., P. Mann, N.R. Grindlay, and J.F. Dolan, James F. (1999), Three-phase

252 tectonic evolution of the northern margin of Puerto Rico as inferred from an
253 integration of seismic reflection, well, and outcrop data, *Mar. Geol.*, 161, 259-288.
254 Varnes, D. J. (1978), Slope movements: Types and processes, in *Landslide analysis and*
255 *control*, edited, pp. 11-33, Transp. Res. Board, Natl. Acad. Sci., Washington D.C.
256 Ward, S. N. (2001), Landslide tsunami, *J. Geophys. Res.*, 106, 11201-11215.

257

258 **Figure Captions:**

259 Figure 1. (a) Perspective view of part of the edge of the carbonate platform north of
260 Arecibo, Puerto Rico. View is to the south. Black polygons – interpreted slope failures.
261 Red lines - locations of seismic reflection profiles that aided with the interpretation of
262 landslides. Inset - Bathymetry map of the northern margin of Puerto Rico [*ten Brink et*
263 *al.*, 2004]. Contour interval is 500 m. Dashed line marks the area of the perspective view.
264 Black lines mark the edges of the tilted carbonate layers. Blue line marks the assumed
265 original northern edge of the carbonate platform before tilting. Arrows mark fissures in
266 the carbonate strata. (b) Migrated seismic reflection profile NAT44 showing cross-
267 section of the modeled landslide. Curved reflectors may represent out-of-plane
268 diffractions. Inset - Interpretation of that landslide used as an input to the hydrodynamic
269 model. Green – Pre-failure profile of the slope. Red – Final profile of the slope following
270 excavation of the upper part of the slope and deposition in the lower part. (c) Perspective
271 view of the bathymetry of a single failure scarp (grey shaded) and the smooth surface that
272 was fit within its perimeter (red lines). The failure volume was calculated by subtracting
273 the scarp bathymetry from the depth of the smooth surface.

274

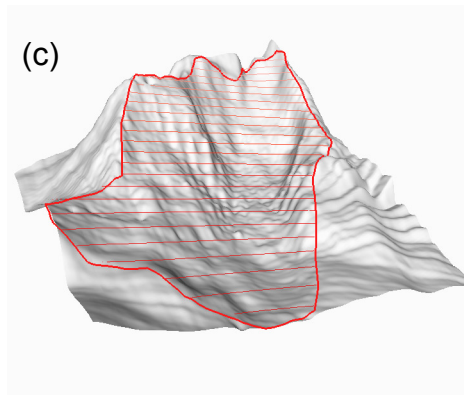
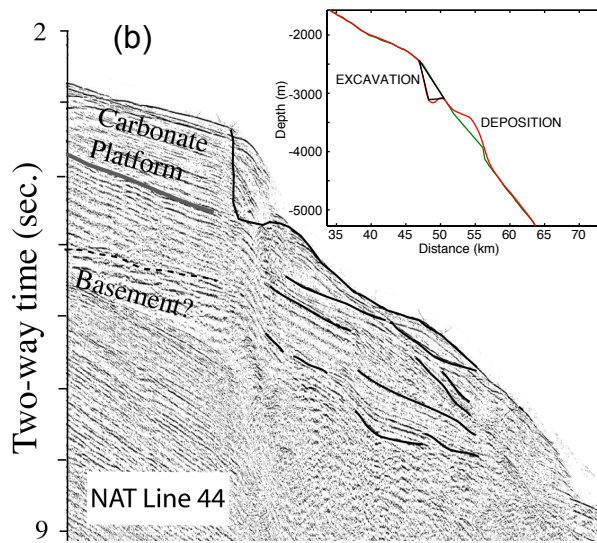
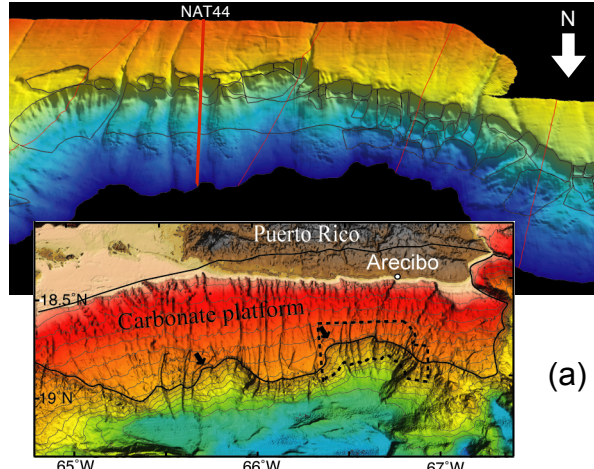
275 Figure 2. Cumulative volume distribution of submarine slope failures north of Puerto
276 Rico. Dots – observations. Line – best fit regression line on a log-log plot.

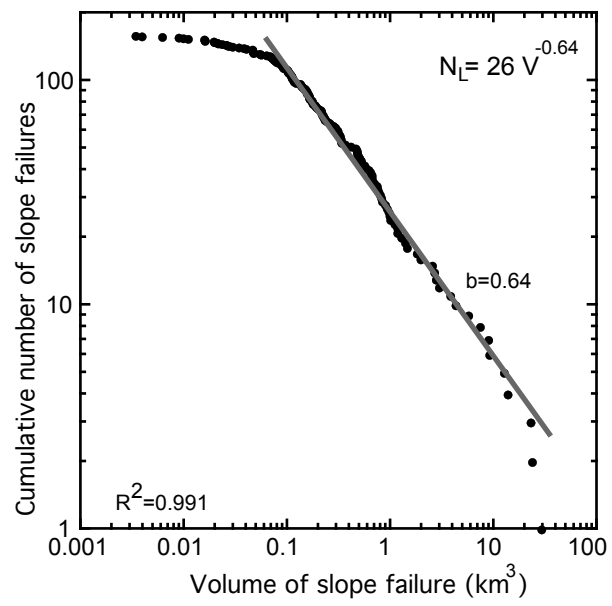
277

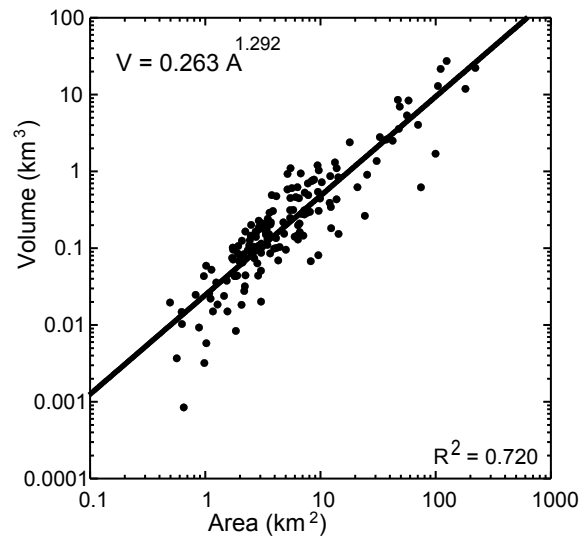
278 Figure 3. Relationship between volume and area of 160 submarine failure scarps along
279 the edge of the carbonate platform (Figure 1).

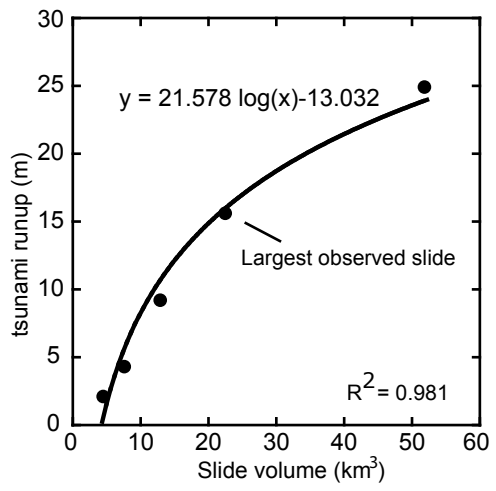
280

281 Figure 4. Maximum tsunami runup on the northern coast of Puerto Rico as a function of
282 landslide volume. The runup was calculated for the largest failure volume, shown in
283 Figure 1b, with an observed width of 22 km, volume of 22 km³, and slide duration of 200
284 s. Other volumes were calculated by keeping the same landslide profile and varying their
285 width (34, 11, 5.5, and 2.25 km).









Details of tsunami modeling

Because of the large vertical motions and shorter wavelengths associated with landslides, nonlinearity and dispersion equations may be more of a concern for landslide-generated tsunamis than for seismogenic tsunamis. When the maximum seafloor displacement is much smaller than the water depth above the slide, then the weakly nonlinear equations [Lynett and Liu, 2002] can be used. Nonlinearity can also be important for accurately determining tsunami run-up, especially for large incident waves. As the tsunami propagates away from the source, frequency dispersion also becomes important. Landslide-generated waves are typically not the long waves characteristic of seismogenic sources, and so energy will be dispersed in the direction of wave propagation as different wave components (frequencies) travel at different velocities according to a dispersion relation (Figure S3; See also Figure 7 in ten Brink et al., 2006). Lynett and Liu [2002] use the arbitrary-level velocity computation [Nwogu, 1993] to "extend" the validity of frequency dispersion for the depth-integrated equations into the intermediate water regime, allowing for accurate simulation of waves with lengths greater than two water depths. The extended weakly non-linear equations are implemented in the program COULWAVE using a finite-difference approximation using a high-order predictor-corrector scheme [Lynett and Liu, 2002]. The spatial grid size used for the computations is 300 m with a time step of 0.3 s. Bottom friction is accounted for with a constant friction factor $f=0.01$ [e.g., Mercado et al., 2002] using the quadratic bottom friction formulation. A moving boundary condition [Lynett et al., 2002] is implemented along the coast to represent run-up and overland flow. For the open-ocean boundary conditions, a sponge-layer absorption scheme is used.

The dynamics of submarine slope failures can only be observed with permanent ocean observatories [e.g., Xu et al., 2004]. Because we model slope failures as regions of progressive depletion and down slope regions of debris accumulation, it is difficult to assign an effective slide speed as with simple block slides commonly used in tsunami studies. We can assign different length scales, such as run-out distance or horizontal displacement of the slide head, to calculate an effective velocity from the slide duration time, t_d . Using an 8 km characteristic length scale for the landslide that spans the area of excavation and deposition (Figure 1b) and $t_d = 200$ s, our effective slide velocity is approximately $8000/200$ or 40 m/s. For comparison, the following velocities were used in tsunami modeling case studies: 75 m/s and 35 m/s for the prehistoric Nuuanu, Hawaii and Storegga, Norway slides, respectively (Ward, 2001), 20-60 m/s for the landslide component of the 1998 Papua New Guinea tsunami (Heinrich et al., 2001), 40-80 m/s for the 1888 Ritter Island volcanogenic tsunami (Ward and Day, 2003), and 25-30 m/s for the Storegga slide (Bondevik et al., 2005).

References:

- Bondevik, S., F. Lovholt, C.B. Harbitz, J. Mangerud, A. Dawson, and J.I. Svendsen, (2005), The Storegga Slide tsunami; comparing field observations with numerical simulations, *Mar. Petrol. Geol.*, 22, 195-208.
- Heinrich, P., A. Piatanesi, and H. Hebert (2001), Numerical modelling of tsunami generation and propagation from submarine slumps; the 1998 Papua New Guinea event, *Geophys. J. Int.*, 145, 97-111.
- Lynett, P., and P. L.-F. Liu (2002), A Numerical Study of Submarine Landslide Generated Waves and Runup, *Proc. Royal Soc. Lond. A.*, 458, 2885-2910.
- Lynett, P., T.-R. Wu, and P. L.-F. Liu (2002), Modeling wave runup with depth-integrated equations, *Coastal Engineering*, 46, 89-107.
- Mercado, A., N.R. Grindlay, P. Lynett, P., and P. L.-F. Liu, (2002), Investigation of the potential tsunami hazard on the north coast of Puerto Rico

due to submarine landslides along the Puerto Rico trench, Report submitted to Puerto Rico State Emergency Management Agency and Sea Grant College Program, 432 pp.

Nwogu, O. (1993), Alternative form of Boussinesq equations for nearshore wave propagation, *J. Waterway, Port, Coastal, Ocean Engineering*, 119, 618-638.

Okal, E. A., and C. E. Synolakis (2004), Source discriminants for near-field tsunamis, *Geophys. J. Int.*, 158, 899-912.

ten Brink, U. S., E.L. Geist, P. Lynett, and B. Andrews (2006), Submarine slides north of Puerto Rico and their tsunami potential, in *Caribbean Tsunami Hazard*, edited by A. Mercado and P. L.-F. Liu, World Scientific Publishing, Hackensack.

Ward, S. N. (2001), Landslide tsunami, *J. Geophys. Res.*, 106, 11201-11215.

Ward, S. N., and S. Day (2003), Ritter Island Volcano; lateral collapse and the tsunami of 1888, *Geophys. J. Int.*, 154, 891-902.

Xu, J. P., M.A. Noble, and L.K. Rosenfeld (2004), In-situ measurements of velocity structure within turbidity currents, *Geophys. Res. Lett.*, 31, doi:10.1029/2004GL019718.

Table 1. Parameters of different model sensitivity runs

slide duration (s)	friction factor	slide runout (km)	propagation time (s)	Grid size for calculation (m)	Slide width (km)	Depletion volume- (km ³)	Accumulation volume- (km ³)	Runup (m)
200	0.01	4.5	800	267	22	21.69	22.30	15.70
200	0.001	4.5	800	267	22			17.30
133	0.01	4.5	800	267	22			24.00
400	0.01	4.5	800	267	22			8.80
200	0.01	6	1200	400	22	20.32	21.28	9.20
200	0.01	4.5	800	300	11	12.54	12.71	9.30
200	0.01	4.5	800	300	5.5	7.22	7.41	4.40
200	0.01	4.5	800	300	2.25	4.23	4.29	2.20
200	0.01	4.5	800	300	34	52.24	51.66	25.00

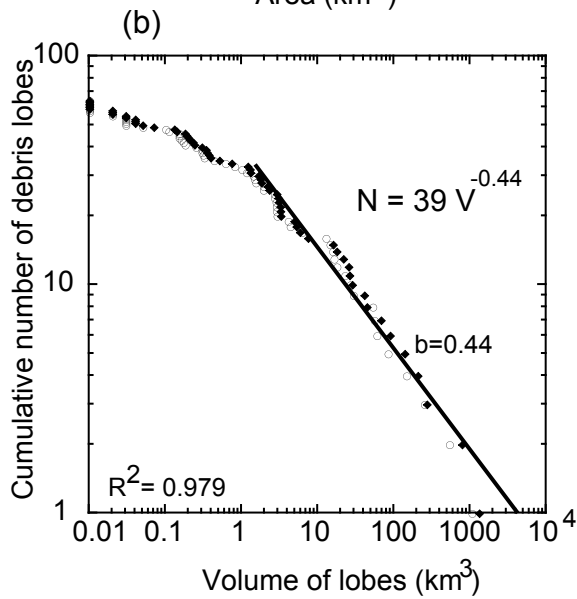
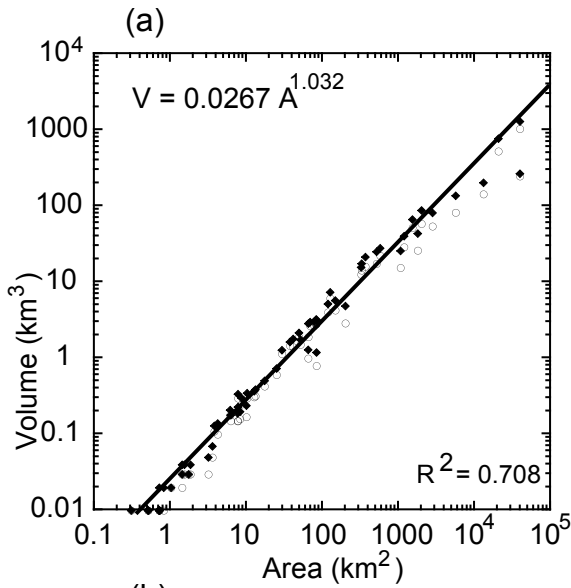


Figure S1. (a) Relationship between volume and area of 63 submarine debris lobes in the Storegga slide (from tabulation by Halfidason et al., 2005). Black diamonds - Maximum volume estimates. Open circles - Minimum volume estimates. Black line - best fit line to the maximum estimates. (b) Cumulative volume distribution of the debris lobes. Symbols as in (a).

Figure S3. Top - Bathymetry of part of the Arecibo amphitheater-shaped scarp and a simple representation of the largest slope failure in the study area (See Figure 1). Yellow region - onshore Puerto Rico. Bottom Maximum wave height calculated by the hydrodynamic simulation during an 800 s model run. Failure duration, $t = 133$ s. Note wave dispersion and a much larger amplitude propagating with the direction of the slide and away from shore.

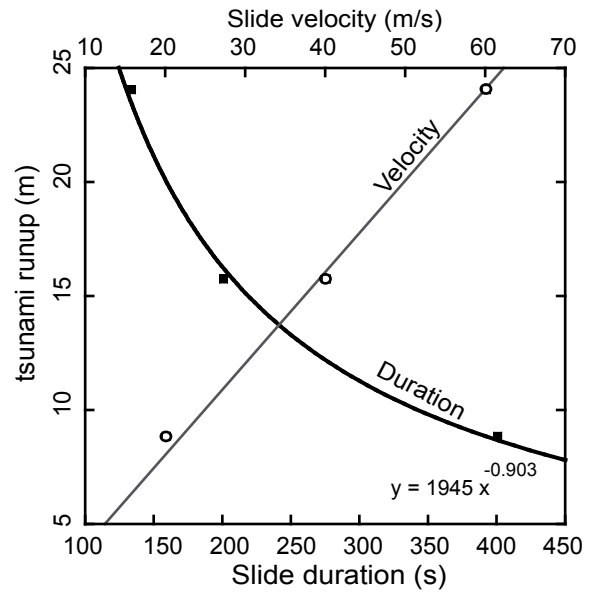
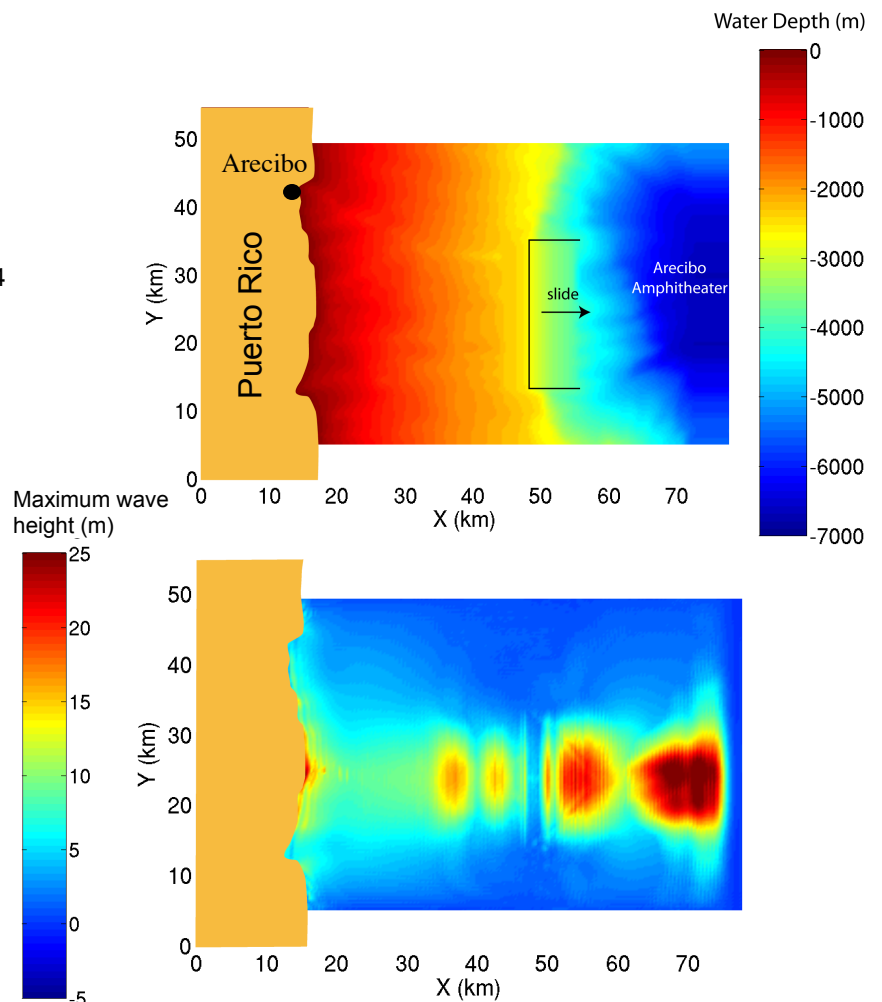


Figure S2. Sensitivity tests showing the dependence of runup calculations on the assumed slide duration and on approximate slide velocity. All tests were calculated for the landslide shown in Figure 1b with a width of 22 km.